Electron affinity measurements of lanthanide atoms: Pr, Nd, and Tb

Xiaoxi Fu,[1] Yuzhu Lu,[1] Rulin Tang,[1] and Chuangang Ning[1,2,*]

[1]*Department of Physics, State Key Laboratory of Low Dimensional Quantum Physics, Tsinghua University, Beijing 100084, China*

[2]*Collaborative Innovation Center of Quantum Matter, Beijing, China*

(Received 4 September 2019; revised manuscript received 22 November 2019; accepted 16 January 2020; published 11 February 2020)

Electron affinities (EAs) of many lanthanide elements still remain unknown due to their complicated electronic structures and relatively low EA values. In the present work, we utilized the slow-velocity map-imaging method combined with an ion trap to resolve conundrums. The EA values of praseodymium, neodymium, and terbium are determined to be 881.0(37) cm^{-1} or 0.109 23(46) eV, 786.3(26) cm^{-1} or 0.097 48(31) eV, and 1059.1(64) cm^{-1} or 0.131 31(79) eV, respectively. We also observed several excited states of Pr, Nd, and Tb anions.

DOI: 10.1103/PhysRevA.101.022502

I. INTRODUCTION

Lanthanides are of profoundly physical and technological significance because of their unique electronic structures. They act as important components of many magnetic materials, catalysts, and superconductors. Recently, atomic anions of lanthanides have aroused the interest of researchers in that there exist electric dipole ($E1$) bound-to-bound transitions in La and Ce anions [1–5], which may pave the way for sympathetically cooling antiprotons [6–9].

Lanthanides, the f-block elements, pose as one of the most challenging groups of elements for electronic structure theory on account of their complex electronic structures, the significant electron correlation effects, and substantial relativistic contributions [10,11]. Unlike other atomic properties, the calculation results of electron affinities (EAs) of lanthanides are of considerable inaccuracy and far from satisfactory. *Ab initio* calculations and semiempirical estimates of the EAs of some lanthanides have been made in the past few years [12–22]. Theoretical calculations have made explicit that the attachment of a $6p$ or $5d$ electron rather than a $4f$ electron has contributed to the formation of lanthanide atomic anions due to the strong correlation effects between $4f$ valence electrons [12,15,17]. Dinov and Beck [23] conducted valence shell relativistic configuration-interaction calculations (RCI) and predicted that Pr^- seemed to be unable to attach either a $5d$ electron or a $4f$ electron. They only found two bound states for the configuration $4f^36s^26p^1$ whose electron affinities were 0.110 eV for $J = 4$ and 0.128 eV for $J = 5$. The $J = 3$ and $J = 6$ states were barely bound when core-valence effects were taken into account. Later, they expanded the methodology of allowing a rotation of the bases within the $4f^n$ subgroup to include the mixing of LS terms from individual neutral J calculations and calculated the EA of Pr to be 0.177 eV [14]. Another five bound states of Pr^- which are formed by the attachments of $6p$ electrons to the Pr ground state $4f^36s^2$ have been presented. After one year, they predicted another bound state of opposite parity which is due to $6s$ attachment to an excited neutral Pr threshold [24]. Cole and Perdew [25] combined the configuration-interaction methods with the local spin-density (LSD) approximation to incorporate correlation effects within an orbital scheme. They predicted that the electron affinities for Pr and Nd are 0.11 and 0.10 eV, respectively, assuming the configuration is the same as that of the neutral atom plus one extra $5d$ electron. However, they were skeptical about the existence of stable Nd^- and Pr^- because their theory tended to exaggerate the affinities for $5d$ electrons. O'Malley and Beck [14] determined the electron affinity of Nd to be 0.167 eV from relativistic configuration-interaction calculations. They treated the $4f^n$ subgroup as corelike electrons with fixed LS terms to cope with the computational complexity of these lanthanide systems. They predicted [13] that the photodetachment channel from the ground state of Nd^- $^6K_{9/2}$ to the Nd $^7K_{4,5}$ threshold had larger detachment cross sections. The $6s$ detachments to excited $4f^46s6p$ states dominated the total detachment cross sections. They also showed the two possibilities of the ground state of Tb^- which differ in parities and electronic configurations [14,15]. They predicted the EA of Tb to be 85 and 88 meV chronologically [14,15]. Felfli *et al.* [26] used their recently developed Regge-pole methodology to calculate the near-threshold electron elastic scattering total and Mulholland partial cross sections and obtained the theoretical EA values of Pr, Nd, and Tb as 0.631, 0.162, and 0.436 eV, respectively. Later, they revised the EA values of Nd and Tb to be 1.88 and 3.04 eV through the scrutiny of the calculated electron scattering total cross sections [27].

On the experimental side, Davis and Thompson [28] determined the EA of Pr to be 0.962(24) eV via laser photodetachment electron spectroscopy. They also reported at least one bound excited state whose binding energy was 0.866(18) eV relative to the ground state of the Pr atom. Apparently, there exists a huge discrepancy between this experimental EA value and the aforementioned theoretical results. Few experimental EA values of Nd and Tb have been reported. The accelerator mass spectrometry only estimated the EA(Nd) to be $\geqslant$50 meV and the EA(Tb)$\geqslant$100 meV [29]. These estimated EA values of Tb and Nd were relatively low which were consistent with the less considerable yields of Tb^- and Nd^- compared to

*ningcg@tsinghua.edu.cn

those of La^- and Ce^- confirmed by the accelerator mass spectrometry [29]. The paucity of experimental measurements can be traced to several factors. Intensities of most lanthanide anion beams are not strong enough for traditional experimental studies without an ion trap [30]. For example, the intensity of Pr^- can be enhanced by a factor of 3 when the ion trap is used. The scarcity of infrared light makes the situation even worse when it is necessary to detach lanthanide anions near the threshold. Moreover, it is challenging to correctly assign the congested and heavily overlapped photoelectron energy spectra obtained with traditional methods due to the complexity of the electronic structures of lanthanides. It is not a surprise that large deviations will emerge due to incorrect assignments. For example, Davis and Thompson measured the electron affinity of cerium to be 0.955(26) eV [31]. However, O'Malley and Beck later revised the EA(Ce) as 0.660 eV via reinterpreting the spectra [12]. This might be the same case for the discrepancy between the theoretical predictions and the EA(Pr) value measured by Davis and Thompson [28].

Recently, we successfully utilized the slow-velocity map-imaging (SEVI) method in combination with a cryogenically controlled ion trap to measure the EA values of transition elements [32–36]. The SEVI method has an outstanding energy resolution of a few cm^{-1} near photodetachment thresholds [37]. Recently, the performance of SEVI has been further improved via the four-plate imaging lens design [38–40]. The introduction of a cryogenically controlled ion trap can effectively enhance intensities of anion beams via accumulations [41–43], which serves as an important feature for those elements with lower EA values. The two advantages have paved the way for measuring EA values and for resolving congested spectra of lanthanides.

II. EXPERIMENTAL SETUP

Our apparatus has been described in detail previously [41]. The experiment has three phases, which are the production, trapping, and photodetachment of anions. Plasmas are generated when the ablation laser (∼10 mJ, 532 nm) is focused on the lanthanide metal disk which is translating and rotating backward and forward. The anions in the plasmas fly through an ion lens and enter the ion trap which is a radio-frequency (rf) octupole trap. The ion trap is mounted on the second stage of a liquid helium refrigerator whose temperature can be controlled from 5 to 300 K. The hot anions lose their kinetic energies due to collisions with the buffer gas in the ion trap. The trapped anions can be efficiently cooled down to ∼10 K. The buffer gas is usually a mixture of H_2 and He with a ratio of 20:80. Pure He and N_2 are occasionally used in certain circumstances [34]. The cooled anions are ejected out via pulsed potentials on the end caps of the ion trap. Later, a −1000-V high-voltage pulse accelerates the anions in the Wiley-McLaren time-of-flight mass spectrometer [44]. The anions of interest are selected via a mass gate and are detected via a microchannel plate (MCP) ion detector. The MCP detector can be moved out of the ion path during the photodetachment phase. Finally, a tunable dye laser detaches the anions in the interaction area of the VMI lens [38,45]. The outgoing electrons are projected onto an MCP enhanced phosphor screen. A charge-coupled device (CCD) camera records raw photoelectron images with an event counting mode. Each image is usually an accumulated result of 50 000 laser shots. The wavelength of the dye laser is monitored in real time via a HighFinesse WS-600 wavelength meter with an accuracy of $0.02\,cm^{-1}$. The maximum-entropy velocity Legendre method [46] is adopted to reconstruct radial and angular distributions of photoelectrons from raw images.

III. RESULTS AND DISCUSSIONS

Figure 1 shows the photoelectron spectrum of Pr^-, which is a result of piecing together two energy distributions at photon energies $h\nu = 14\,731.64$ and $15\,397.30\,cm^{-1}$. Peaks ranging from 37 to 43 in Fig. 1 are acquired at photon energy $15\,397.30\,cm^{-1}$, and the rest are acquired at photon energy $14\,731.64\,cm^{-1}$. This is a very complicated spectrum. To assign so many peaks, we changed the buffer gas and trapping time to observe their different changing trends of peak intensities. Figures 2 and 3 refer to the energy spectra accumulated with varied buffer gases and trapping time at two photon energies. Peak 1 is attributed to the EA transition with certainty. Therefore, the intensity of peak 1 is used for the normalization of different energy spectra for better comparisons. Intensities of peaks originating from anionic excited bound states will rise when trapping time is shortened due to the higher survival chance. Their intensities will also rise as the buffer gas is switched from the mixture of H_2 and He to pure He because H_2 can quench excited states more effectively [34]. Peaks from the same initial state should manifest a similar changing trend in distinct circumstances. Peaks 8, 9, 15, 33, and 42 evolve consistently with peak 1 at first glance. Therefore, these peaks should be assigned to photodetachment channels from the ground state of Pr^-. The intensities of prominent peaks 4, 5, 6, and 12 change dramatically when the trapping condition is altered. Besides, their trends are in accord with those of peaks 2, 3, 7, 11, 14, and 17. Therefore, those peaks are related to the same anionic excited state. As shown in Fig. 3(b), there is an emerging peak emerging adjacent to peak 1 when the trapping time is set to be 5 ms at a lower photon energy $h\nu = 11\,603.40\,cm^{-1}$. Peak 0 is the sign of another anionic excited state.

Since the energy levels of neutral atom Pr [47] are well known with high accuracy, they serve as fingerprints to settle the final states of peaks with the same initial states. The selection rules of photodetachment have been considered for the determinations of the terms of these three anionic states. In view of the calculated results by Beck [14] and the selection rules of photodetachment [48], we concluded that $^5K_5$ is the ground state of Pr^- and the first excited state is $^5I_4$. The configurations of the final neutral states of observed peaks from the anionic second excited state are $4f^25d6s^2$, $4f^25d^26s$, and $4f^35d6s$. If the configuration of the second excited state is $4f^36s^26p$, two electrons located at the $4f$ and $6p$ shells both have to change to reach the final states with a configuration $4f^25d^26s$, which will have a much smaller photodetachment cross section. Moreover, the total angular momentum quanta J of almost all assigned final states are equal to 13/2 or 11/2 and those of S are equal to 6 or 4. In addition, the lifetime of $^5L_6$ was predicted as 14 min [24]; it can survive after being stored

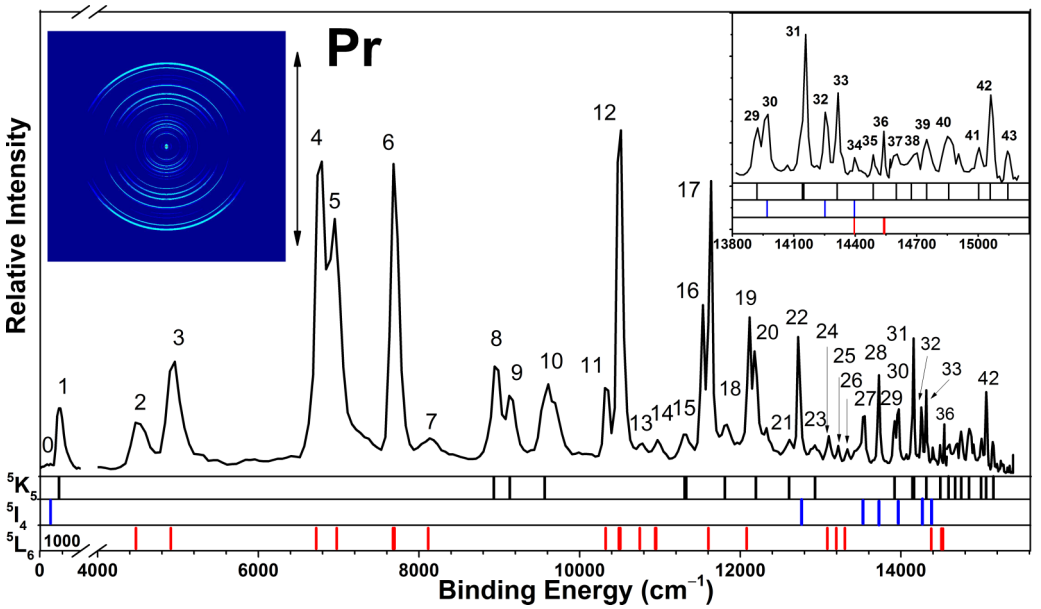

FIG. 1. Photoelectron energy spectra of Pr^- obtained through two energy spectra at $h\nu = 14\,731.64\,cm^{-1}$ and $15\,397.30\,cm^{-1}$ pieced together for a better view. The sets of sticks below the spectrum indicate the energy levels of the final neutral states of photodetachment channels from the same anionic states labeled on the left side. The black sticks are for the transitions from the anionic ground state $^5K_5$, blue for the first excited state $^5I_4$, and red for the second excited state $^5L_6$. The photoelectron image at the top left is obtained at $h\nu = 14\,731.64\,cm^{-1}$. The double arrow corresponds to the polarization of the photodetachment laser. The inset at the top right is an expanded view for peaks 29–43.

in the ion trap for 45 ms. As mentioned above, the second excited states are assigned to be $^5L_6$ with the configuration $4f^25d^26s^2$.

Among those peaks from the ground state, the binding energy of peak 33 lies within the tuning range of our dye laser. To determine its binding energy more accurately, we scanned the photon energy from 14 481.65 to 14 781.31 cm^{-1} slightly above the photodetachment threshold with a step of 50 cm^{-1}. Since the ejected photoelectrons with the same kinetic energy form a spherical shell and are projected onto the screen as a ring, the radius of the ring will be proportional to the velocity of the photoelectrons. As shown in Fig. 4, the experimental data plotted with $h\nu$ versus r^2 form a line. The binding energy of peak 33 is determined via the intercept of the fitted line on account of the relation $h\nu = BE + \alpha r^2$ where α is the energy calibration coefficient. Thus, the binding energy of transition $Pr(^6K_{9/2}) \leftarrow Pr^-(^5K_5)$ is $14\,313.5(37)\,cm^{-1}$. The uncertainty has included the laser linewidth of $0.06\,cm^{-1}$. By subtracting the energy level $13\,432.52\,cm^{-1}$ [47] of the final state $^6K_{9/2}$ from $14\,313.5(37)\,cm^{-1}$, the EA value of

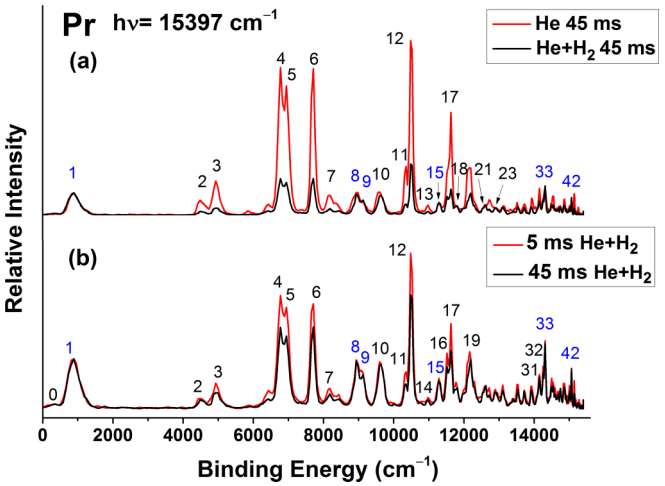

FIG. 2. Photoelectron spectra of Pr^- obtained with different buffer gases (a) and different trapping times (b) at the photon energy $15\,397\,cm^{-1}$. Peaks 1, 8, 9, 15, 33, and 42 have the same trend as the experimental conditions change. They are all related to the transitions from the anionic ground state $^5K_5$.

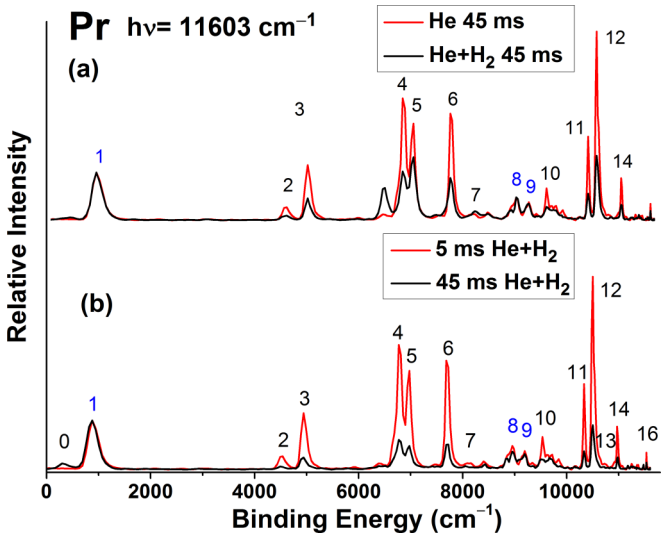

FIG. 3. Photoelectron spectra of Pr^- obtained with different buffer gases (a) and different trapping times (b) at the photon energy $= 11\,603\,cm^{-1}$.

TABLE I. Measured binding energies and assigned binding energies of the transitions for Pr^- observed in the present work.

Peaks	Levels (Pr ← Pr^-)	Measured binding energy (cm^{-1})	Assigned binding energy (cm^{-1})[a]
0	$^4I_{9/2} \leftarrow {}^5I_4$	362(171)	529(2)
1	$^4I_{9/2} \leftarrow {}^5K_5$	867(26)	881(4)
2	$^4I_{9/2} \leftarrow {}^5L_6$	4501(19)	4495(5)/
3	$^4K_{11/2} \leftarrow {}^5L_6$	4925(16)	4929(5)
4	$^6L_{11/2} \leftarrow {}^5L_6$	6743(25)	6777(10)
5	$^2H_{11/2} \leftarrow {}^5L_6$	6926(26)	6956(5)
6	$^4G_{7/2} \leftarrow {}^5L_6/{}^6L_{13/2} \leftarrow {}^5L_6$	7682(10)	7680(5)/7693(5)
7	$^6L_{11/2} \leftarrow {}^5L_6$	8131(181)	8143(5)
8	$^6L_{11/2} \leftarrow {}^5K_5$	8948(9)	8961(4)
9	$^6K_{9/2} \leftarrow {}^5K_5$	9132(9)	9131(4)
10	$^6L_{13/2} \leftarrow {}^5K_5$	9612(9)	9614(4)
11	$^4H_{13/2} \leftarrow {}^5L_6$	10328(9)	10329(5)
12	$^4L_{13/2} \leftarrow {}^5L_6/{}^4K_{11/2} \leftarrow {}^5L_6$	10491(6)	10486(5)/10494(5)
13	$^6L_{17/2} \leftarrow {}^5L_6$	10758(15)	10783(10)
14	$^4K_{11/2} \leftarrow {}^5L_6/{}^4H_{9/2} \leftarrow {}^5L_6$	10967(13)	10967(5)/10983(5)
15	$^4L_{13/2} \leftarrow {}^5K_5/{}^4K_{11/2} \leftarrow {}^5K_5$	11311(5)	11305(4)/11313(4)
16		11529(4)	
17	$^6I_{13/2} \leftarrow {}^5L_6$	11625(4)	11626(5)
18	$^6I_{9/2} \leftarrow {}^5K_5$	11795(14)	11818(8)
19	$^6I_{13/2} \leftarrow {}^5L_6$	12104(5)	/
20	$^6I_{11/2} \leftarrow {}^5K_5$	12179(10)	12164(8)
21	$^4K_{13/2} \leftarrow {}^5K_5$	12608(13)	12627(8)
22	$^6I_{11/2} \leftarrow {}^5I_4$	12724(37)	12709(3)
23	$^6I_{13/2} \leftarrow {}^5K_5$	12917(11)	12933(8)
24	$^6I_{11/2} \leftarrow {}^5L_6$	13099(3)	13099(5)
25	$^6I_{13/2} \leftarrow {}^5L_6$	13216(3)	13209(5)
26	$^6I_{9/2} \leftarrow {}^5L_6$	13330(3)	13335(5)
27	$^4K_{15/2} \leftarrow {}^5I_4$	13535(3)	13531(2)
28	$^6L_{21/2} \leftarrow {}^5I_4$	13723(3)	13727(1)
29	$^6I_{11/2} \leftarrow {}^5K_5$	13918(1)	13917(4)
30	$^6K_{9/2} \leftarrow {}^5I_4$	13965(2)	13961(3)
31	$^6I_{9/2} \leftarrow {}^5K_5/{}^4L_{17/2} \leftarrow {}^5K_5$	14155(2)	14161(4)/14154(4)
32	$^6I_{11/2} \leftarrow {}^5I_4$	14256(1)	/
33	$^6K_{9/2} \leftarrow {}^5K_5$	14314(1)	14313(4)
34	$^4K_{17/2} \leftarrow {}^5L_6/{}^6I_{7/2} \leftarrow {}^5I_4$	14399(2)	14403(5)/14396(1)
35	$^6I_{9/2} \leftarrow {}^5K_5$	14488(2)	14487(4)
36	$^6I_{9/2} \leftarrow {}^5L_6/{}^6I_{13/2} \leftarrow {}^5L_6$	14538(2)	14531(5)/14533(5)
37	$^6I_{11/2} \leftarrow {}^5K_5$	14592(8)	14608(8)
38	$^6I_{9/2} \leftarrow {}^5K_5$	14699(18)	14703(4)
39	$^6I_{11/2} \leftarrow {}^5K_5$	14749(2)	14753(4)
40	$^6I_{9/2} \leftarrow {}^5K_5$	14857(2)	14856(4)
41	$^6I_{9/2} \leftarrow {}^5K_5$	15004(6)	15020(12)
42	$^6I_{9/2} \leftarrow {}^5K_5$	15062.98(55)	15067(4)
43	$^6I_{9/2} \leftarrow {}^5K_5$	15146(1)	15154(8)

[a]Deduced values obtained by additions of the measured binding energies of the anionic states and the energy levels of neutral Pr according to our listed assignments.

Pr is determined to be 881.0(37) cm^{-1} or 0.109 23(46) eV. Note that 1 eV = 8065.543 937 cm^{-1}, as recommended by 2018 CODATA [49]. Our result is significantly lower than the previous result 0.962(24) eV reported by Davis and Thompson [28]. The reason for the big discrepancy is not clear. One possible explanation is that the most prominent feature (peaks 4–6) was incorrectly assigned as the transition from the anionic ground state to the neutral ground state in their photoelectron energy spectrum. If peaks 4 and 6 corresponded to those two peaks observed by Davis and Thompson, the EA of Pr would be 0.954(3) eV and the binding energy of the bound state would be 0.838(3) eV based on their incorrect assignment. These two values are consistent with their values 0.962(24) and 0.866(18) eV [28]. Our result does not match the theoretical value 0.631 eV reported by Felfli *et al.* [26] well. It should be pointed out that our result is in agreement with the theoretical predictions 0.128 and 0.177 eV reported by Beck [14,23]. Since the energy levels of the neutral Pr atomic states [47] which can be taken as the fingerprints for the assignment are well known with high accuracy, all observed peaks in Fig. 1 are reliably assigned. See details in Table I. The peak in the same row with "/" is selected as the

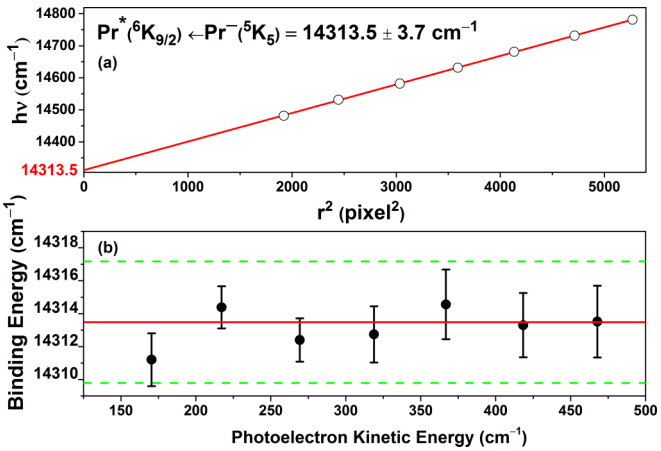

FIG. 4. The photon energy $h\nu$ versus r^2 for transition 33. The solid line is the linear least-squares fitting. The intercept 14 313.5 cm^{-1} is the binding energy of transition 33 (a). The binding energy of transition $Pr(^6K_{9/2}) \leftarrow Pr^-(^5K_5)$ as a function of the kinetic energy of photoelectrons. The dashed lines indicate the uncertainty $\pm 3.7\,cm^{-1}$ (b).

one to determine the binding energy of its original state. As a result, its "measured binding energy" and "assigned binding energy" will be numerically equal, so the value of "assigned binding energy" will be omitted. Two excited bound states of Pr^- were observed and their binding energies, deduced from the binding energies of peaks 32 and 19, are determined to be 0.065 59(25) eV for $^5I_4$ and 0.007 81(62) eV for $^5L_6$.

Figure 5 shows the photoelectron energy spectrum of Nd^- at photon energy $h\nu = 15\,397.36\,cm^{-1}$. The intensity of the atomic anion Nd^- signal is very weak in the mass spectra. The pure He gas was used as the buffer gas instead of 80%He + 20%H_2 since we found that Nd^- reacts with H_2 gas readily even at a temperature as low as 10 K. As shown by the vertical sticks under the spectrum, most of the peaks can be assigned to the states of Nd^- except the band located at the binding energy region from 6000 to 9000 cm^{-1}. Since the NdH^- signal is much stronger than Nd^- in the mass spectra, contamination caused by NdH^- is a likely explanation for this unexpected band. Nd has seven isotopes, i.e., $m = 142(27\%)$, 143 (12%), 144 (24%), 145 (8%), 146 (17%), 148 (6%), 150 (6%). To check this possibility, we also measured the photoelectron energy spectra of NdH^-. The spectra of Nd^- were acquired as the anions with mass number $m = 142$ were selected and photodetached. The spectra of $^{142}NdH^-$ were acquired when species with a mass of 143 were photodetached. It should be pointed out that there is a tiny contribution of $^{143}Nd^-$ for spectra of $m = 143$. However, the intensity of $^{143}Nd^-$ beams is much weaker than that of $^{142}NdH^-$ beams. As shown in Fig. 6, the unexpected band might be due to an unknown species with the same mass number 142 rather than NdH^-. Since the pure He gas cannot effectively cool molecular anions [34], we also used N_2 gas as the buffer gas. To avoid the condensation of N_2 gas, the temperature of the ion trap was kept at 90 K. As the signal intensity of Nd^- was weak and unstable, and it gradually decayed during periods of experiments, it took us almost ten times as much time as for Pr

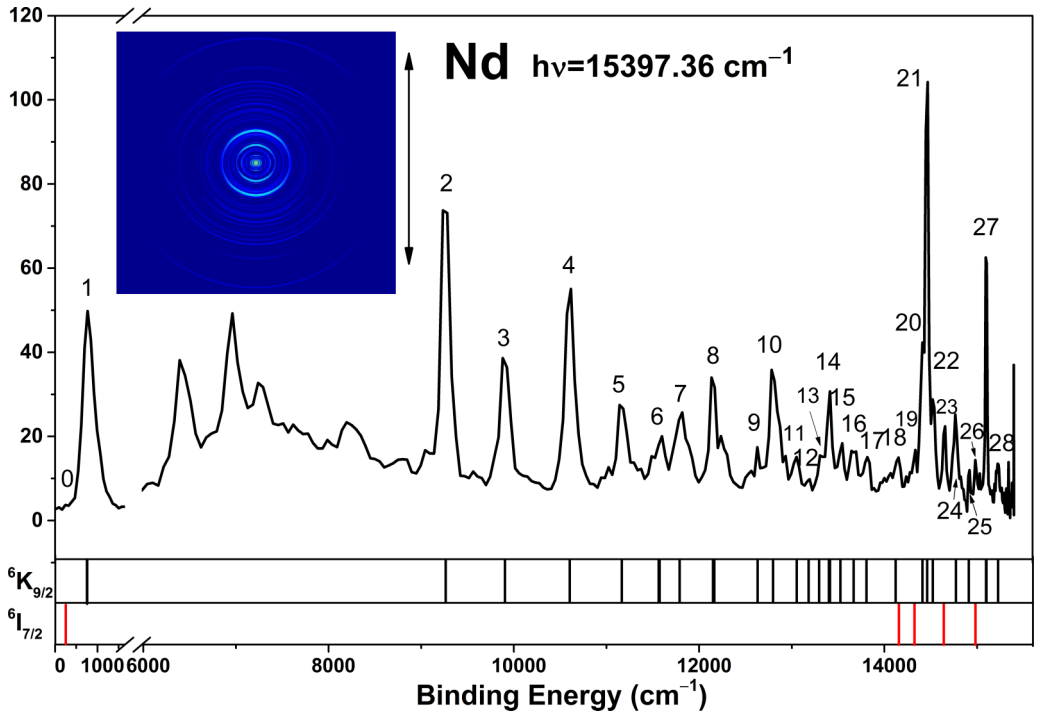

FIG. 5. Photoelectron energy spectra of Nd^-. The sets of sticks below the spectrum indicate the energy levels of the final neutral states of photodetachment channels from the same anionic states labeled on the left side. The black sticks are for the transitions from the anionic ground state $^6K_{9/2}$, and red for the excited state $^6I_{7/2}$. The inset shows the photoelectron image. The double arrow corresponds to the polarization of the photodetachment laser.

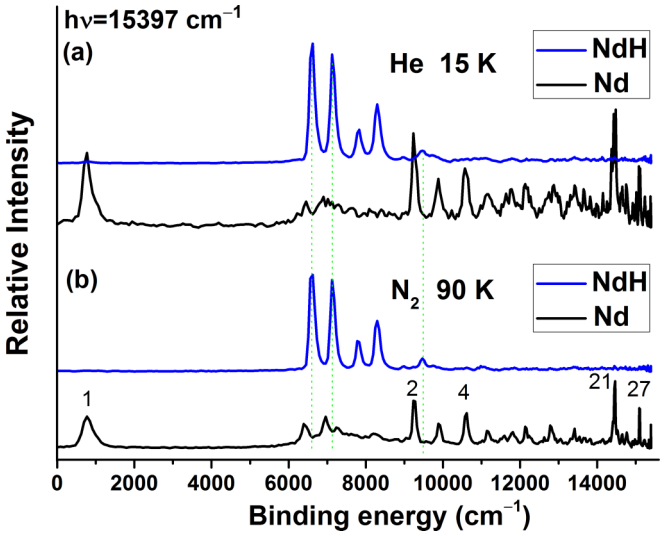

FIG. 6. Comparison of photoelectron spectra of Nd^- [the black (lower) line] and NdH^- [the blue (upper) line] obtained with the buffer gas He (a) and N_2 (b) and the trapping time is 45 ms. The dotted lines are used for guiding the eyes.

to obtain a spectrum like Fig. 5. Therefore, we could not scan a photodetachment threshold with a fine step as we did for Pr.

We use the strongest peak 21 to determine the EA value of Nd. Peak 21 is attributed to the transition from $^6K_{9/2}$ to $^7K_4$. This is consistent with Beck's prediction that this transition had a dramatically large photodetachment cross section [13], which serves as strong evidence for our EA assignment. The binding energy of peak 21 is measured as 14 459.1(26) cm^{-1} via a Gaussian function fitting. Therefore, the electron affinity of Nd is determined to be 786.3(26) cm^{-1} or 0.097 49(32) eV after subtracting the energy level 13 672.851 cm^{-1} of the final state $^7K_4$ [47]. All the assignments of peaks in Fig. 5 are summarized in Table II. It should be pointed out that the L, S, and J quantum numbers of the final neutral states of all assignments also support Beck's prediction [13,14] where $^6K_{9/2}$ was the ground state of Nd^-. The theoretical predictions 0.167 and 0.169 eV by Beck [13,14] and the result 0.162 eV by Felfli *et al.* [26] are slightly higher than our experimental result, and the value 1.88 eV by Felfli *et al.* [27] is not consistent with our experimental result. Our measured values can be taken as benchmarks for developing theoretical models for lanthanides. One excited bound state of Nd^- was also observed and several peaks are supposed to be from this excited state as indicated by the red sticks under the spectrum. In Fig. 5, peak 23 is the most prominent among those peaks which are supposed from the excited state of Nd anions. Since the binding energy of the excited state must be lower than

TABLE II. Measured binding energies and assigned binding energies of the transitions for Nd^- observed in the present work.

Peaks	Levels (Nd ← Nd^-)	Measured binding energy (cm^{-1})	Assigned binding energy (cm^{-1})[a]
0	$^5I_4 \leftarrow {}^6I_{7/2}$	239(59)	209(2)
1	$^5I_4 \leftarrow {}^6K_{9/2}$	793(54)	786(3)
2	$^7L_5 \leftarrow {}^6K_{9/2}$	9259(18)	9262(3)
3	$^7L_6 \leftarrow {}^6K_{9/2}$	9903(16)	9901(3)
4	$^7K_4 \leftarrow {}^6K_{9/2}$	10603(13)	10601(3)
5	$^7K_5 \leftarrow {}^6K_{9/2}$	11169(12)	11163(3)
6	$^5L_6 \leftarrow {}^6K_{9/2}/{}^7M_8 \leftarrow {}^6K_{9/2}$	11574(14)	11561(3)/11571(3)
7	$^7I_3 \leftarrow {}^6K_{9/2}$	11804(22)	11788(3)
8	$^7K_4 \leftarrow {}^6K_{9/2}/{}^5G_3 \leftarrow {}^6K_{9/2}$	12149(10)	12147(3)/12162(3)
9	$^7G_1 \leftarrow {}^6K_{9/2}$	12630(25)	12628(3)
10	$^7K_5 \leftarrow {}^6K_{9/2}$	12805(9)	12796(3)
11	$^7G_3 \leftarrow {}^6K_{9/2}$	13041(10)	13051(3)
12	$^5H_5 \leftarrow {}^6K_{9/2}$	13189(40)	13181(3)
13	$^5I_6 \leftarrow {}^6K_{9/2}$	13320(61)	13292(3)
14	$^7G_4 \leftarrow {}^6K_{9/2}/{}^7L_4 \leftarrow {}^6K_{9/2}$	13407(11)	13410(3)/13398(3)
15	$^5H_3 \leftarrow {}^6K_{9/2}$	13530(6)	13523(3)
16	$^7I_4 \leftarrow {}^6K_{9/2}$	13667(7)	13665(3)
17	$^5I_4 \leftarrow {}^6K_{9/2}$	13810(7)	13803(3)
18	$^5L_8 \leftarrow {}^6K_{9/2}/{}^7K_9 \leftarrow {}^6I_{7/2}$	14137(21)	14120(3)/14163(5)
19	$^5I_5 \leftarrow {}^6I_{7/2}$	14328(14)	14332(2)
20	$^7H_2 \leftarrow {}^6K_{9/2}$	14407(4)	14408(3)
21	$^7K_4 \leftarrow {}^6K_{9/2}$	14459(3)	/
22	$^7H_3 \leftarrow {}^6K_{9/2}$	14524(4)	14520(3)
23	$^7I_3 \leftarrow {}^6I_{7/2}$	14648(2)	/
24	$^7H_4 \leftarrow {}^6K_{9/2}$	14765(2)	14769(3)
25	$^5I_5 \leftarrow {}^6K_{9/2}$	14912(6)	14909(3)
26	$^7I_8 \leftarrow {}^6I_{7/2}$	14986(4)	14989(2)
27	$^5H_6 \leftarrow {}^6K_{9/2}/{}^7K_5 \leftarrow {}^6K_{9/2}$	15099.4(9)	15094(6)/15098(3)
28	$^7I_3 \leftarrow {}^6K_{9/2}$	15221(2)	15225(3)

[a]Deduced values obtained by additions of the measured binding energies of the anionic states and the energy levels of neutral Nd according to our listed assignments.

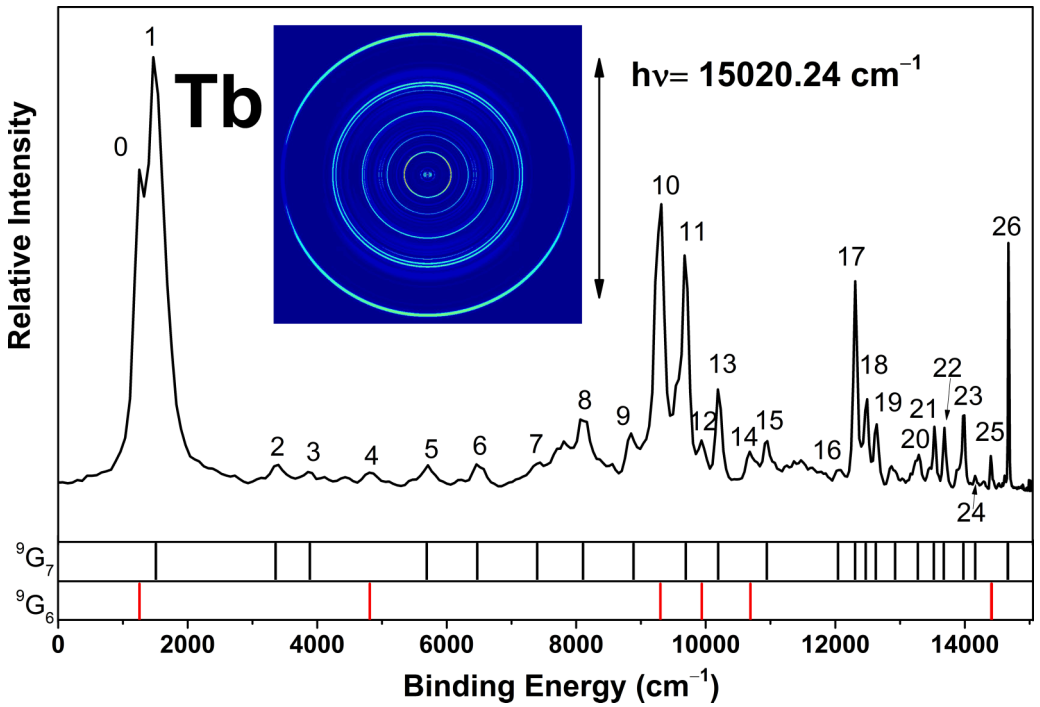

FIG. 7. Photoelectron energy spectra of Tb^- obtained at the photon energy = 15 020.24 cm^{-1} with the trapping time of 45 ms and H_2 + He as the buffer gas. The sets of sticks below the spectrum indicate the energy levels of the final neutral states of photodetachment channels from the same anionic states labeled on the left side. The inset shows the photoelectron image obtained with trap-on mode and the trapping time is 45 ms. The double arrow corresponds to the polarization of the photodetachment laser.

EA and the energy level of its final state must be lower than the binding energy of peak 23 itself, we can infer reasonably its final state will range from 13 896.372 to 14 466.980 cm^{-1}. Terms with electronic configuration $4f^46s6p$ whose energy levels lie within this range are only $^5K_7$ and $^7I_3$. Considering the excited state is $4f^46s^26p$ predicted by Beck [13,14] and the ejected electron should be detached directly with no more electrons changing state, the electronic configuration of the final state should be $4f^46s6p$. However, if we assign its final state as $^5K_7$ (14 311.994 cm^{-1}), there will be no choice for the final state of peak 26. As a result, the final state of peak 23 is assigned to $^7I_3$. The final states of peaks 18, 19, and 26 are also determined to be $^7K_9$, $^5I_5$, and $^7I_8$, respectively. It is worth mentioning that the configuration of these three final states is $4f^45d6s$. That is to say, one electron is detached from the 6*s* shell and another electron needs to change from the 6*p* shell to the 5*d* shell, which enjoys a smaller cross section compared to that of direct detachment of the 6*s* shell. These assignments agree with the fact that peak 23 is much stronger than peaks 18, 19, and 26. Therefore, we tend to assign the excited state of Nd^- to be $^6I_{7/2}$ rather than $^4H_{7/2}$ in spite of Beck's prediction [13] that they have the same cross section when they are detached to $^7I_3$. Beck predicted that the detachment channels from $^6I_{7/2}$ or $^4H_{7/2}$ to $^7I_3$ both had a relatively large cross section [13].The binding energy of excited bound state $^6I_{7/2}$ is measured to be 209(2) cm^{-1} according to the binding energy of peak 23.

Figure 7 shows the photoelectron spectra of Tb^-. All observed peaks can be assigned with two initial states of the atomic anion Tb^- after carefully comparing the positions of the peaks with the energy levels of the neutral atom Tb. Beck predicted that Tb^- has six bound states of odd parity: $4f^85d^16s^26p^1$ $^9G_7$, $^9G_6$, $^9G_8$, $^9G_5$, $^7F_6$, and $^7G_7$ in energy increasing order [15], and two bound states of even parity: $4f^96s^26p^1$ $^7H_8$ and $^7H_7$ [14]. The lowest state of odd parity is $^9G_7$ whose binding energy is calculated to be 88 meV [15] and the lowest state of even parity is $^7H_8$ whose binding energy is 85 meV [14]. Since the final states of peaks 0

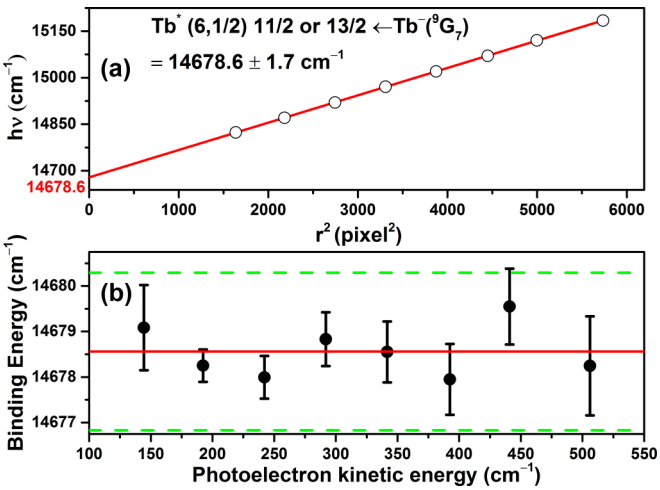

FIG. 8. The photon energy $h\nu$ versus r^2 for transition 26. The solid line is the linear least-squares fitting. The intercept 14 678.6 cm^{-1} is the binding energy of transition 26 (a). The binding energy of transition $Tb^*\{(6, 1/2)J = 11/2$ or $J = 13/2\} \leftarrow Tb^-(^9G_7)$ as a function of the kinetic energy of photoelectrons. The dashed lines indicate an uncertainty ±1.7 cm^{-1} (b).

TABLE III. Measured binding energies and assigned binding energies of the transitions for Tb^- observed in the present work.

Peaks	Levels (Tb ← Tb^-)	Measured binding energy (cm^{-1})	Assigned binding energy (cm^{-1})[a]
0	$^8G_{15/2} \leftarrow {}^9G_6$	1225(36)	1251(6)
1	$^8G_{15/2} \leftarrow {}^9G_7$	1481(38)	1518(6)
2	$^8D_{11/2} \leftarrow {}^9G_7$	3385(15)	3366(6)
3	$^8G_{9/2} \leftarrow {}^9G_7$	3866(21)	3896(12)
4	$^8G_{1/2} \leftarrow {}^9G_6$	4823(15)	4807(6)
5	$^8H_{17/2} \leftarrow {}^9G_7$	5707(12)	5703(6)
6	$^8H_{15/2} \leftarrow {}^9G_7$	6492(12)	6481(6)
7	$^8H_{13/2} \leftarrow {}^9G_7$	7418(37)	7408(6)
8	$^6G_{13/2} \leftarrow {}^9G_7$	8118(15)	8116(6)
9	$^8H_{7/2} \leftarrow {}^9G_7$	8873(13)	8896(12)
10	$^{10}G_{17/2} \leftarrow {}^9G_6$	9288(7)	9295(6)
11	$^{10}G_{11/2} \leftarrow {}^9G_7$	9678(15)	9702(12)
12	$^{10}G_{9/2} \leftarrow {}^9G_6$	9926(7)	9934(6)
13	$^{10}G_{9/2} \leftarrow {}^9G_7$	10200(4)	10201(6)
14	$^{10}D_{9/2} \leftarrow {}^9G_6$	10692(11)	10686(6)
15	$^{10}D_{9/2} \leftarrow {}^9G_7$	10946(10)	10954(6)
16	$^6H_{11/2} \leftarrow {}^9G_7$	12063(6)	12054(6)
17	$^{10}F_{11/2} \leftarrow {}^9G_7$	12311(3)	12316(6)
18	$^{10}F_{13/2} \leftarrow {}^9G_7$	12476(5)	12482(6)
19	$^{10}F_{15/2} \leftarrow {}^9G_7$	12633(6)	12637(6)
20	$^{10}H_{9/2} \leftarrow {}^9G_7$	13270(11)	13284(6)
21	$^8G_{13/2} \leftarrow {}^9G_7$	13533(3)	13532(6)
22	$^{10}H_{15/2} \leftarrow {}^9G_7$	13686(3)	13685(6)
23	$^8G_{15/2} \leftarrow {}^9G_7$	13982(2)	13989(6)
24	$^8G_{13/2} \leftarrow {}^9G_7$	14161(2)	14172(12)
25	(6,1/2) 11/2← $^9G_6$/(6,1/2) 13/2← $^9G_6$	14405(2)	/
26	(6,1/2) 11/2← $^9G_7$/(6,1/2) 13/2← $^9G_7$	14676.7(3)	14672(6)/14678(6)

[a]Deduced values obtained by additions of the measured binding energies of the anionic states and the energy levels of neutral Tb according to our listed assignments.

and 1 are $4f^8(^7F)5d^16s^2\ ^8G_{15/2}$, we tentatively assign the electron configuration of initial states as the state of odd parity $4f^85d^16s^26p^1$. The reason is that direct photodetachment of a $6p$ electron usually favors a larger cross section than photodetachment of a $6p$ electron with another electron excited from $5d$ to $4f$ simultaneously. Furthermore, the working conditions with buffer gas 80%He + 20%H_2 and trapping time 45 ms can effectively quench the excited states if there is an allowed electric dipole transition ($E1$). Therefore, it is reasonable to assign the ground state of Tb^- as $4f^85d^16s^26p^1\ ^9G_7$, and the first excited state as $4f^85d^16s^26p^1\ ^9G_6$. These assignments have considered the above-mentioned selection rules and still need further theoretical confirmation. The strong sharp peak 26 is chosen for the measurement of the EA value of Tb. We scanned the photon energy from 14 823.47 to 15 184.23 cm^{-1} with a step of 50 cm^{-1} to accurately determine the binding energy of peak 26. The final states of peak 26 may include two neutral states $4f^8(^7F_6)6s^26p_{1/2}$ with $(6, 1/2)^o J = 11/2$ at 13 616.27 cm^{-1} and $(6, 1/2)^o J = 13/2$ at 13 622.69 cm^{-1} [47]. As shown in Fig. 8, the binding energy of peak 26 is determined to be 14 678.6 cm^{-1}. At the current stage, we cannot resolve these two photodetachment channels. Therefore, the uncertainty of the electron affinity of Tb is limited to the energy interval between these two neutral states. The EA value of Tb is determined to be 1059.1(64) cm^{-1} or 0.131 31(79) eV. The binding energy of the first excited state $^9G_6$ is measured to be 789(6) cm^{-1} in light of the binding energy of peak 25. Our value is in good agreement with the theoretical

TABLE IV. The summary of EA values of Pr, Nd, and Tb, and binding energies of their anionic bound states obtained in the present work.

Ln[a]	EAs (cm^{-1})/(eV)	Configuration of Ln^-	Bound state of Ln^-	Binding energy (cm^{-1})
Pr	881.0 (37)/0.10923(46)	$4f^36s^26p^1$	$^5K_5$	881.0(37)
		$4f^36s^26p^1$	$^5I_4$	529(2)
		$4f^25d^26s^2$	$^5L_6$	63(5)
Nd	786.3(26)/0.09749(32)	$4f^46s^26p^1$	$^6K_{9/2}$	786.3(26)
		$4f^46s^26p^1$	$^6I_{7/2}$	209(2)
Tb	1059.1(64)/0.13131(79)	$4f^85d^16s^26p^1$	$^9G_7$	1059.1(64)
		$4f^85d^16s^26p^1$	$^9G_6$	789(6)

[a]Means lanthanides.

results 0.085 and 0.088 eV presented by Beck [14,15] but not consistent with the values 0.436 or 3.04 eV predicted by Felfli *et al.* [26,27]. All the assignments are summarized in Table III.

In conclusion, the electron affinities of Pr, Nd, and Tb are measured to be 881.0(37) cm^{-1} or 0.109 23(46) eV, 786.3(26) cm^{-1} or 0.097 49(32) eV, and 1059.1(64) cm^{-1} or 0.131 31(79) eV, respectively. The measured EA values of Pr, Nd, and Tb, and binding energies of bound excited states of their anions are summarized in Table IV. The demonstrated ability to resolve complicated electronic structures via the slow-electron velocity map-imaging method in combination with a cold ion trap presents a clear path forward in measurements of electron affinities and congested electronic states of lanthanides and actinides.

ACKNOWLEDGMENTS

This work is supported by the National Natural Science Foundation of China (NSFC) (Grants No. 91736102 and No. 11974199) and the National Key R&D Program of China (Grants No. 2018YFA0306504).

[1] L. Pan and D. R. Beck, Phys. Rev. A **82**, 014501 (2010).
[2] C. W. Walter, N. D. Gibson, D. J. Matyas, C. Crocker, K. A. Dungan, B. R. Matola, and J. Rohlen, Phys. Rev. Lett. **113**, 063001 (2014).
[3] C. W. Walter, N. D. Gibson, C. M. Janczak, K. A. Starr, A. P. Snedden, R. L. Field III, and P. Andersson, Phys. Rev. A **76**, 052702 (2007).
[4] C. W. Walter, N. D. Gibson, Y.-G. Li, D. J. Matyas, R. M. Alton, S. E. Lou, R. L. Field III, D. Hanstorp, L. Pan, and D. R. Beck, Phys. Rev. A **84**, 032514 (2011).
[5] Y. Z. Lu, R. L. Tang, X. X. Fu, and C. G. Ning, Phys. Rev. A **99**, 062507 (2019).
[6] G. Cerchiari, A. Kellerbauer, M. S. Safronova, U. I. Safronova, and P. Yzombard, Phys. Rev. Lett. **120**, 133205 (2018).
[7] A. Kellerbauer and J. Walz, New J. Phys. **8**, 45 (2006).
[8] E. Jordan, G. Cerchiari, S. Fritzsche, and A. Kellerbauer, Phys. Rev. Lett. **115**, 113001 (2015).
[9] P. Yzombard, M. Hamamda, S. Gerber, M. Doser, and D. Comparat, Phys. Rev. Lett. **114**, 213001 (2015).
[10] M. Dolg. *Computational Methods in Lanthanide and Actinide Chemistry* (John Wiley & Sons Ltd, Chichester, UK, 2015).
[11] W. J. Cao, D. Hewage, and D. S. Yang, J. Chem. Phys. **148**, 044312 (2018).
[12] S. M. O'Malley and D. R. Beck, Phys. Rev. A **74**, 042509 (2006).
[13] S. M. O'Malley and D. R. Beck, Phys. Rev. A **77**, 012505 (2008).
[14] S. M. O'Malley and D. R. Beck, Phys. Rev. A **78**, 012510 (2008).
[15] S. M. O'Malley and D. R. Beck, Phys. Rev. A **79**, 012511 (2009).
[16] S. M. O'Malley and D. R. Beck, Phys. Rev. A **61**, 034501 (2000).
[17] S. H. Vosko and J. A. Chevary, J. Phys. B: At., Mol. Opt. Phys. **26**, 873 (1993).
[18] E. Eliav, U. Kaldor, and Y. Ishikawa, Phys. Rev. A **52**, 291 (1995).
[19] A. Borschevsky, E. Eliav, M. J. Vilkas, Y. Ishikawa, and U. Kaldor, Eur. Phys. J. D **45**, 115 (2007).
[20] B. Karaçoban and L. Özdemir, Chin. J. Phys. **50**, 40 (2012).
[21] S. M. O'Malley and D. R. Beck, Phys. Rev. A **60**, 2558 (1999).
[22] L. Pan and D. R. Beck, Phys. Rev. A **93**, 062501 (2016).
[23] K. Dinov and D. R. Beck, Phys. Rev. A **51**, 1680 (1995).
[24] S. M. O'Malley and D. R. Beck, Phys. Rev. A **81**, 032503 (2010).
[25] L. A. Cole and J. P. Perdew, Phys. Rev. A **25**, 1265 (1982).
[26] Z. Felfli, A. Z. Msezane, and D. Sokolovski, Phys. Rev. A **79**, 012714 (2009).
[27] Z. Felfli and A. Z. Msezane, J. At., Mol., Condens. Nano Phys. **5**, 73 (2018).
[28] V. T. Davis and J. S. Thompson, J. Phys. B: At., Mol. Opt. Phys. **35**, L11 (2002).
[29] M.-J. Nadeau, M. A. Garwan, X.-L. Zhao, and A. E. Litherland, Nucl. Intrum. Methods **B123**, 521 (1997).
[30] C. S. Feigerle, R. R. Corderman, S. V. Bobashev, and W. C. Lineberger, J. Chem. Phys. **74**, 1580 (1981).
[31] V. T. Davis and J. S. Thompson, Phys. Rev. Lett. **88**, 073003 (2002).
[32] R. L. Tang, X. L. Chen, X. X. Fu, H. Wang, and C. G. Ning, Phys. Rev. A **98**, 020501(R) (2018).
[33] X. L. Chen and C. G. Ning, J. Phys. Chem. Lett. **8**, 2735 (2017).
[34] R. L. Tang, X. X. Fu, Y. Z. Lu, and C. G. Ning, J. Phys. Chem. Lett. **10**, 702 (2019).
[35] Z. H. Luo, X. L. Chen, J. M. Li, and C. G. Ning, Phys. Rev. A **93**, 020501(R) (2016).
[36] X. X. Fu, Z. H. Luo, X. L. Chen, J. M. Li, and C. G. Ning, J. Chem. Phys. **145**, 164307 (2016).
[37] D. M. Neumark, J. Phys. Chem. A **112**, 13287 (2008).
[38] I. León, Z. Yang, H. T. Liu, and L. S. Wang, Rev. Sci. Instrum. **85**, 083106 (2014).
[39] D. Townsend, M. P. Minitti, and A. G. Suits, Rev. Sci. Instrum. **74**, 2530 (2003).
[40] M. L. Weichman, J. A. DeVine, D. S. Levine, J. B. Kim, and D. M. Neumark, Proc. Natl. Acad. Sci. USA **113**, 1698 (2016).
[41] R. L. Tang, X. X. Fu, and C. G. Ning, J. Chem. Phys. **149**, 134304 (2018).
[42] X. B. Wang and L. S. Wang, Rev. Sci. Instrum. **79**, 073108 (2008).
[43] C. Hock, J. B. Kim, M. L. Weichman, T. I. Yacovitch, and D. M. Neumark, J. Chem. Phys. **137**, 244201 (2012).
[44] W. C. Wiley and I. H. McLaren, Rev. Sci. Instrum. **26**, 1150 (1955).
[45] A. T. J. B. Eppink and D. H. Parker, Rev. Sci. Instrum. **68**, 3477 (1997).

[46] B. Dick, Phys. Chem. Chem. Phys. **16**, 570 (2014).

[47] J. E. Sansonetti and W. C. Martin, J. Phys. Chem. Ref. Data **34**1559 (2005).

[48] P. C. Engelking and W. C. Lineberger, Phys. Rev. A **19**, 149 (1979).

[49] E. Tiesinga, P. J. Mohr, D. B. Newell, and B. N. Taylor, The 2018 CODATA internationally recommended values of the fundamental physical constants (Web Version 8.0). Database developed by J. Baker, M. Douma, and S. Kotochigova. Available at http://physics.nist.gov/constants, National Institute of Standards and Technology, Gaithersburg, (2019).